Effects of Track Structure on the Ion Radiolysis of the Fricke Dosimeter

Simon M. Pimblott* and Jay A. LaVerne

Radiation Laboratory, University of Notre Dame, Notre Dame, Indiana 46556-0579

Received: March 28, 2002; In Final Form: July 11, 2002

The chemistry of the Fricke dosimeter induced by low and high linear energy transfer (LET) radiation has been modeled using the stochastic IRT method, incorporating simulated ion tracks. Comparison of the results for track segments with experimentally determined differential yields shows excellent agreement for energetic electrons, and for nonrelativistic ions, including ^{1}H, ^{4}He, ^{12}C, and ^{20}Ne. There is a significant effect of particle type and energy on the response of the Fricke dosimeter, which reflects the competition between intra-track reaction of the radiation-induced radicals, diffusion, and scavenging. This competition is modified by changes in the ion track structure. Monte Carlo track structure simulations show that the radial energy loss profiles are similar for ions with the same velocity/charge ratio and that ∼40% of the energy is initially deposited within a water diameter of the track axis. The LET of the ionizing radiation is shown to be a poor parameter for characterizing the Fricke dosimeter and the observed chemistry is predicted more precisely by the square of the ratio of the particle charge to its velocity.

Introduction

Stochastic diffusion−kinetic modeling has proven to be a great help in understanding the early events occurring in the radiolysis of water by fast electrons,[1−6] but similar calculations for heavy ion radiolysis are only now becoming possible. The physical track of a heavy ion, and therefore the radiation-induced chemistry, is very different than that of a fast electron because of the much higher rate of linear energy transfer, LET (= $-dE/dx$, the stopping power).[7] The development of radiation chemical models of heavy ion radiolysis using sophisticated diffusion-kinetic calculations coupled with realistic descriptions of the physics of ion tracks require a large computing capacity. The accuracy of these models is best determined by comparing their predictions with experimental data on well-characterized chemical systems that have been examined with a wide variety of incident radiation particles and energies. One of the most studied systems in radiation chemistry is the Fricke dosimeter, which has been examined with primary particles ranging from protons to uranium ions.[8−10] Successful prediction of the observed radiation chemistry will enhance the validity of a model for the various physical aspects of the radiation track structure and support its ability to elucidate the early radiation chemical events.

The Fricke dosimeter is an aerated solution of 1−10 mM $FeSO_4$ in aqueous 0.4 M H_2SO_4. It is straightforward to prepare and it provides an easy quantification of the energy deposited by ionizing radiation. The chemistry is based upon the oxidation of Fe(II) ions to Fe(III) by the oxidizing species $^{\bullet}OH$, $HO_2^{\bullet}$, and H_2O_2 that are produced in the radiolytic decomposition of water

$$Fe(II) + {}^{\bullet}OH \rightarrow Fe(III) + OH^- \quad k = 4.3 \times 10^8\ M^{-1}s^{-1} \quad (1)$$

$$Fe(II) + H_2O_2 \rightarrow Fe(III) + {}^{\bullet}OH + OH^- \quad k = 42\ M^{-1}s^{-1} \quad (2)$$

$$Fe(II) + HO_2^{\bullet} \rightarrow Fe(III) + H_2O_2 + OH^- \quad k = 2.1 \times 10^6\ M^{-1}s^{-1} \quad (3)$$

The rate coefficients used throughout this work are from the compilation of Buxton et al.[11] The radiation-induced reducing radicals, e_{aq}^- and $^{\bullet}H$, are rapidly converted to $HO_2^{\bullet}$ under the aerated conditions of the Fricke dosimeter by the following reactions

$$H_3O^+ + e_{aq}^- \rightarrow {}^{\bullet}H \quad k = 2.3 \times 10^{10}\ M^{-1}s^{-1} \quad (4)$$

$$^{\bullet}H + O_2 \rightarrow HO_2^{\bullet} \quad k = 2.1 \times 10^{10}\ M^{-1}s^{-1} \quad (5)$$

Consequently, the yield of oxidized equivalents, i.e., Fe(III), is given by the following stoichiometric equation

$$G(Fe(III)) = G({}^{\bullet}OH) + 2\,(G(H_2O_2)) + 3\,(G(e_{aq}^-) + G({}^{\bullet}H) + G(HO_2^{\bullet}))$$

Radiation chemical yields are given in G-values, with the unit of the number of molecules or radicals produced per 100 eV of energy absorbed.

The Fricke dosimeter is the only radiation chemical system that has received systematic study using low-LET radiations, that is energetic electrons and γ-rays,[12−14] and using high-LET radiations, such as accelerated ions[8] and neutrons.[15] The limiting yield of the Fricke dosimeter, obtained with fast electrons and ^{60}Co γ-rays, is G(Fe(III)) = 15.6 ions/100 eV. Lower yields are obtained for low-energy electrons[12] and for light and heavy ions.[8] The variation in the ferric ion yield is due to the intra-track chemistry of the radical species because of differences in the relative spatial distribution of the reactants within the geometry of the track structure. Therefore, the observed chemistry in conjunction with the model calculations can be used to probe the physical track structure.

This study addresses the effect of particle type and energy on the chemistry and the yield of the Fricke dosimeter, so as to elucidate the effects of track structure in radiolysis. In the following section, the stochastic simulation techniques used to model the radiation-induced chemistry are described briefly. The

10.1021/jp020830u CCC: $22.00
Published on Web 09/25/2002

results are presented and discussed in the third section. A summary is presented and conclusions are drawn in the final section.

Methodology

A number of different deterministic and stochastic techniques have been developed for modeling the radiation chemistry of water and aqueous solutions.[2,16−18] These methods have been critiqued in the past,[19] and it has been demonstrated that the most realistic approach involves the stochastic diffusion-kinetic modeling of the evolution of simulated track structures.[20] This type of treatment explicitly takes into account the identities and the nonhomogeneous spatial distribution of the radiation-induced reactants. The calculations reported here follow the methodology outlined in ref 21, and in refs 4 and 5 for track structure simulation and stochastic diffusion kinetic modeling, respectively.

Track Structure Simulation. As a radiation particle passes through an aqueous solution, it is attenuated, transferring energy to the molecular electrons and causing ionizations and excitations. The trajectory of an ionizing radiation particle is modeled collision-by-collision, using an energy-dependent inelastic collision cross-section derived from the dipole oscillator strength distribution of liquid water following the methods originally suggested by Ashley[22] and by Green at al.[23] and using an energy-dependent elastic collision cross-section appropriate for gaseous water. The outcome of an energy-transfer event—ionization or excitation—is determined from the energy dependent ionization efficiency for liquid water.[24−26] When an ionization event occurs, the trajectory of the ejected, secondary electron is followed until it has degraded in energy to less than 25 eV. At this point, the chance of a further ionization event is limited. The effects of low-energy electrons (<25 eV) are included empirically using spatial distributions derived from data obtained from simulations of the attenuation of low-energy electrons in water ice[27] employing experimental ice phase cross-sections.[28,29] Trajectory deviations due to ionization events are determined by classical kinematics, whereas those due to elastic events are determined from the experimental differential cross-section for gaseous water. In the calculations for energetic ions, the attenuation of the primary particle is followed until the initial energy has dropped by 10−150 keV. As this study considers track segments and hence differential yields, it is important that the energy and the energy loss properties of the primary radiation particle do not change significantly in the simulation.

The formalism proposed by Ashley and Green et al. describes the rate of energy loss by a primary particle due to inelastic collisions, but does not incorporate the effects of electron capture and loss by the primary ions. The energy dependences of the effective charge, Z_{eff}, of ^{1}H, ^{4}He, ^{12}C, ^{20}Ne, and ^{58}Ni ions evaluated using the approach of Bloom and Sauter[30] are shown in Figure 1. At the energies considered in the chemistry studies of LaVerne and Schuler[8] and of Appleby et al.,[31] charge cycling processes are not significant for $^{1}H^{+}$, $^{4}He^{2+}$, and $^{20}Ne^{10+}$; they are only relevant at energies less than 20 MeV for ^{12}C. However, the use of an effective charge is important for ^{58}Ni. At 20 MeV, Z_{eff}/Z is 0.93 for ^{12}C, while at 200 MeV Z_{eff}/Z is 0.72 for ^{58}Ni.

Physicochemical Processes. After the transfer of energy from the radiation particle and its daughter electrons to the molecular electrons, all of the ionization events are assumed to result in the production of a geminate ($H_2O^{+}-e^{-}$) pair, whereas a nonionizing electronic excitation is presumed to result in the production of an excited singlet water molecule, which can dissociate into an (H−OH) pair or an ($H_2-O(^{1}D)$) pair, or alternatively undergo nonradiative decay back to ground-state

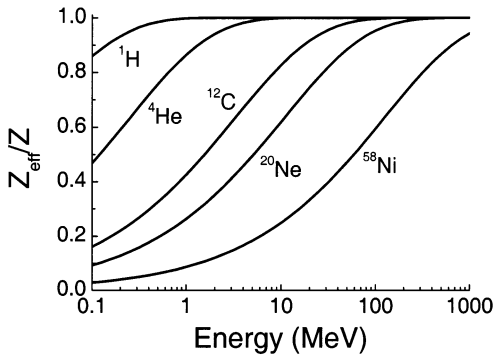

Figure 1. Energy dependences of the effective charge, Z_{eff}, of ^{1}H, ^{4}He, ^{12}C, ^{20}Ne and ^{58}Ni ions evaluated using the approach of Bloom and Sauter.[30]

water. Track structure simulation provides the yields of ionization events and of nonionizing excitation events. The consequences of nonionizing excitation are parametrized to match the known initial yields in the fast electron radiolysis of neutral water taking into consideration available information from photochemical studies,[32,33] following the approach described in ref 34.

Diffusion-Kinetic Modeling. In the following studies, the independent reaction times (IRT) technique[35] is employed to model the competition between the diffusive relaxation of the nonhomogeneous spatial distribution of radiation-induced species and their diffusion-limited reaction. The IRT simulation of diffusion-limited kinetics starts from the initial positions of the radiation-induced reactants furnished by a track structure simulation. These positions are used to determine which pairs of particles are initially in a reactive configuration. The overlapping pairs are allowed to react and, where appropriate, products are generated. A random reaction time is generated for each surviving pair using the independent pairs approximation by sampling from the appropriate first passage time distribution function. Random reaction times are determined for the reaction of each reactive species with the solvent and with the added solutes. The minimum of the ensemble of reaction times comprising the three sets of times—intra-track, solvent, and solute—is the time of the first reaction. The effects of this reaction are tabulated, and new reaction times are generated if appropriate. The minimum of the new ensemble of times is the next reaction time. This procedure continues until a predefined cutoff time is attained. The kinetics of $10^2 - 10^3$ different tracks are simulated to obtain statistically significant information. In most kinetic studies, the cutoff time is usually chosen to be ∼1 μs; however, in modeling the Fricke dosimeter, the slow reaction of H_2O_2 with Fe(III), $k = 42\ M^{-1}s^{-1}$,[11] requires the use of a longer time, ∼1 s. This change also increases the CPU time necessary for simulation. The reaction parameters and diffusion coefficients used in the simulations reported here were obtained from the compilations of Buxton et al.[11] using the treatment outlined in ref 36.

Results and Discussion

The majority of the radiation chemistry experiments performed with energetic ions have measured the track average or integral yield (usually denoted G_o) for the complete energy attenuation of the ion. These yields represent significant changes in the energy loss properties of the primary ion and in the structure of the radiation track. To understand and elucidate the effect of track structure on radiation chemistry, it is more straightforward to consider the sections of an ion track over

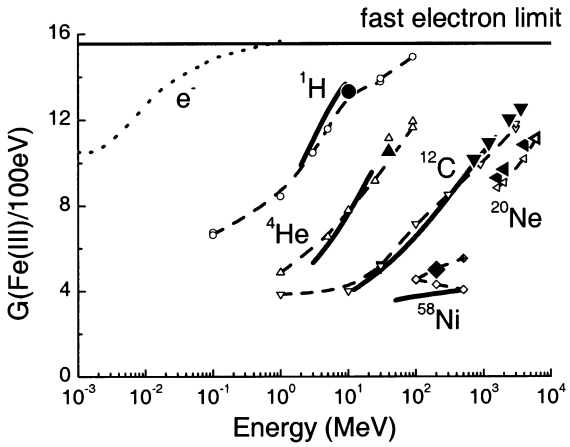

Figure 2. Effect of particle energy on the track segment yield of the Fricke dosimeter. Experimental yields: LaVerne and Schuler[8] (——) labeled curves for ^{1}H, ^{4}He, ^{12}C and ^{58}Ni ions; Sauer et al.[37] (●) ^{2}D(at *E/2*), (▲) $^{4}He^{2+}$; Christmann et al. [31] (▼) ^{12}C, (solid isosceles triangle left) ^{20}Ne. Yield inferred from radial dose distribution: Furukawa et al.[47] (◆). IRT simulations employing simulated track structures: (- - -) e^{-} (track average yield), (○) ^{1}H, (△) ^{4}He, (▽) ^{12}C, (open isosceles triangle left) ^{20}Ne, (◇) $^{58}Ni^{28+}$, (◈) $^{58}Ni^{Zeff+}$. All heavy ion yields joined by (− − −).

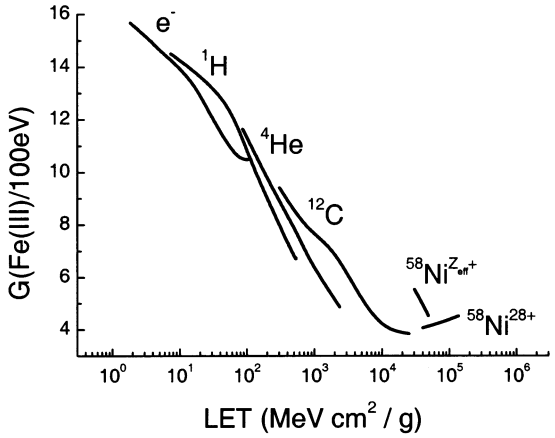

Figure 3. Effect of particle LET on the track segment yield of the Fricke dosimeter. IRT simulations employing simulated track structures: (——) labeled curves for e^{-}, ^{1}H, ^{4}He, ^{12}C and ^{58}Ni.

which the primary ion energy loss properties do not change significantly. Radiation chemical measurements have been made on the Fricke dosimeter for a wide variety of ions, and over a range of energies. LaVerne and Schuler have used this wealth of experimental information to determine the differential (or instantaneous) yields, G_i, of track segments as a function of ion kinetic energy, E, for the irradiation of the Fricke dosimeter with ^{1}H, ^{4}He, ^{12}C, and ^{58}Ni ions.[8] These data and other track segment yields from the literature [31,37] are shown in Figure 2. The experimental data show that for a given ion, the amount of Fe(III) produced decreases as the energy of the radiation particle decreases. The maximum yield of the Fricke dosimeter is ~15.6 and is found for energetic electrons, and the ion energy required to give a specific yield of Fe(III) production increases with ion mass, i.e., $e^{-} < {}^{1}H < {}^{4}He < {}^{12}C < {}^{20}Ne < {}^{58}Ni$. Also included in Figure 2 are stochastic IRT predictions of track average yields for energetic e^{-} and track segment yields for ^{1}H, ^{4}He, ^{12}C, ^{20}Ne, and $^{58}Ni^{28+}$ ion tracks. The simulations for the four lighter ions are in excellent agreement with the experimental track segment yields over the range of ion energies studied experimentally. There is, however, some discrepancy between the experimental data and the calculations for $^{58}Ni^{28+}$ radiolysis. The simulations cover a range of energies greater than that experimentally probed for ^{1}H, ^{4}He, and ^{12}C ions, and the results suggest that the yields of the Fricke dosimeter for light ions tend to the fast electron limit at high ion energies. The minimum differential yield of Fe(III) is different for each ion decreasing in the order $e^{-} > {}^{1}H > {}^{4}He > {}^{12}C > {}^{58}Ni$, with minima in the G(Fe(III)) values found at lower energies than have been probed experimentally (except for ^{58}Ni). The existence of a minimum G(Fe(III) value for energetic electrons has already been suggested.[38,39] In addition, recent experimental studies measuring single strand breaks induced in dilute aqueous solutions of DNA plasmids using X-ray sources of various energies have demonstrated a minimum yield at about 1−2 keV.[40] Assuming a direct correspondence between the OH radical yield and the yield of DNA single strand breaks, this minimum implies a minimum OH radical yield for energetic electron irradiation in this energy range.

It is frequently desirable to have an empirical parameter to use in the description of the radiation chemical effect of track structure. Historically, the effects of radiation quality have been parametrized in terms of the linear energy transfer (LET) of the radiation to the medium.[41] This quantity is numerically equivalent to the stopping power of the medium for radiation particles under the conditions examined here. It has been demonstrated experimentally that LET is an inappropriate descriptor for radiation chemical effects.[8,31,42,43] Figure 3 shows the results of stochastic diffusion kinetic calculations for the dependence of the ferric ion yield on LET for ^{1}H, ^{4}He, ^{12}C, ^{20}Ne, and ^{58}Ni ions. The calculations support the experimental observation that LET is not a unique parameter for predicting the response of the Fricke dosimeter. In general, an increase in the LET leads to a decrease in ferric ion yields. This decrease is about a factor of 4 over the range of LET. The reason for the failure of LET as a descriptive parameter for radiation quality in radiation chemistry is apparent upon closer scrutiny of the structure of ion tracks. The experimental and theoretical studies of the Fricke dosimeter summarized in Figures 2 and 3 focus on ion energies greater than the energy corresponding to the Bragg peak of the appropriate stopping power curves. Parameters affecting the energy loss properties of energetic ions in this domain have been discussed at length.[44] The approach used here for determining the energy loss of the primary heavy ion in liquid water is based on the formalism of Ashley,[22] and Green et al.[23] Comparison of stopping powers calculated for energetic electrons and for ^{1}H, ^{2}D, ^{4}He, and ^{12}C ions in liquid water demonstrates that there is a significant effect of both ion energy and ion type on the rate of energy transfer to the molecular electrons of the water. The charge of the ion also affects the stopping power. With decreasing ion charge, the magnitude of the stopping power decreases for a given velocity. It is well-known that when the energy dependences of the stopping powers for two ions with the same charge, e.g., $^{1}H^{+}$ and $^{2}D^{+}$, are compared in terms of the specific energy (ion energy per mass unit), the two curves are the same. A similar scaling for ions of the same specific energy, but of different charge, reveals that the stopping powers are scaled by a constant multiplier, which is the square of the ion charge, Z^2. In fact, according to Bethe theory,[45] the stopping power of an energetic ion A^{Z+} with mass M and kinetic energy E is approximately equal to Z^2 times that of a proton of energy E/M.

Energy loss distributions, which show the frequency of a given energy loss event from the incident ion to a molecular electron as a function of that energy, exhibit little dependence on ion type and ion energy, suggesting that a given energy loss event is equally probable for any of the ions examined here. The observed differences in the rate of energy transfer for the

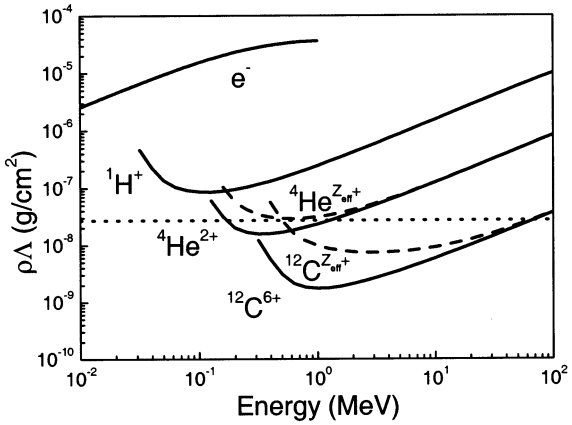

Figure 4. Energy dependence of the mean free path of e^-, $^1H^+$, $^4He^{2+}$ and $^{12}C^{6+}$ in liquid water (——). The effect of charge cycling on the inelastic mean free path is shown by the (− − −) lines for ^4He and ^{12}C. The approximate diameter of a water molecule in liquid water is given by the (••••) line.

different ions reflect the fact that the distances, i.e., mean free paths, between stochastic energy transfer events differ. As the stopping power of an ion increases, the separation between events decreases. It is this inter-event separation along the primary ion path that determines the axial structure of an ion track and ultimately affects the observed chemistry. The radiation chemistry reflects the competition between the diffusive relaxation of the nonhomogeneous spatial distribution of radiation-induced reactants, their intra-track reactions with each other, and their reactions with solutes (scavengers).

The energy dependences of the mean free paths between inelastic events for ^1H, ^4He, and ^{12}C ions are shown in Figure 4. At a given energy, the mean separation between primary inelastic collisions decreases with increasing mass of the radiation particle. However, the separation between primary energy loss events is not the only factor determining the effect of radiation quality on radiation chemistry. It does not provide information about the effects of secondary, delta electrons. The mean free path between primary events is less than the diameter of a water molecule, ~0.27 nm, for low energy, high Z particles. The probability for two energy loss events within the same molecule becomes very high within this regime. However, such an outcome is just an artifact of using a continuum model for ion transport. Techniques that avoid using a continuous medium are more appropriate when the LET is high, and the mean free path is small. For the majority of the calculations performed here, the mean free path is larger than the size of a water molecule, and so the track structures do not involve multiple events on the same molecule. There is one exception, the tracks of ^{58}Ni ions of energy 100−400 MeV, which is discussed separately later.

By combining the primary energy loss events with those from the secondary electrons, it is possible to obtain the instantaneous radial energy deposition rate, which is related to the initial spatial distribution of water decomposition products perpendicular to the trajectory of the primary ion. The instantaneous radial energy deposition profiles for $^1H^+$ ions in liquid water over the energy range 0.2−20 MeV are shown in Figure 5. (The profiles each integrate to one, and so are mathematically strictly densities.) There is a large spike in the vicinity of the primary particle due to the primary ionization and excitation events, and then there is an immediate drop (on the sub-nanometer distance scale). Following the drop from the primary track, there is a spatially extended distribution of energy deposition due to the secondary, ejected electrons. The maximum of the distribution due to the

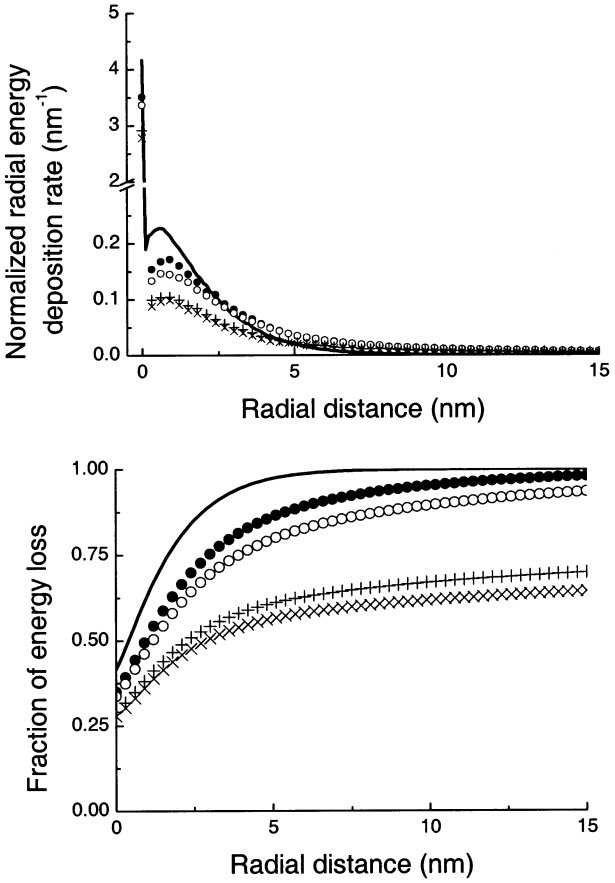

Figure 5. Radial energy deposition profile for ^1H ions in liquid water over the energy range 0.2−20 MeV. (——) 0.2 MeV, (●) 0.5 MeV, (○) 1 MeV, (+) 10 MeV, (×) 20 MeV.

secondary electrons occurs at 0.4−0.7 nm. It is about 5% of the height of the spike due the primary ion. The height of the maximum decreases and the distance to the maximum increases as the energy of the primary ion increases. The distribution due to the secondary electrons has a very long tail, the extent of which decreases as the primary ion energy decreases because of a decrease in the maximum energy of ejected secondary electrons. The extent of the distributions is best demonstrated by integrating the radial energy deposition profiles to give the fraction of the energy within a specified distance of the primary track. For a 0.2 MeV $^1H^+$ ion, almost all, 97%, of the energy is contained within 5 nm of the primary track, which is about the width of the hydrated electron thermalization distribution in water. In contrast, for 10 MeV and 20 MeV proton tracks more than 29% and 33%, respectively, of the energy deposition occurs further than 20 nm from the primary track. The radial energy deposition distributions of these latter two proton tracks are influenced significantly by the trajectories of the ejected, high-energy secondary electrons. A 20 MeV proton can produce secondary electrons of energy up to ~44 keV and with a mean path length of almost 5 μm.[21] These electrons are not very probable; however, when produced they undergo considerable scattering, and they make a significant contribution to the widening of the radial distribution. Figure 6 compares the instantaneous radial energy deposition profile for a 1 MeV $^1H^+$ in liquid water with $^4He^{2+}$ ions of the same LET ($E \approx 27$ MeV) and of the same velocity, i.e., the same specific energy ($E = 4$ MeV or 1 MeV/amu). The profiles for the $^1H^+$ and $^4He^{2+}$ ions of the same LET are very different, but the profiles for ions with the same velocity are similar. Thus, in the radial direction, the track structure of a $^1H^+$ ion more resembles that of a $^4He^{2+}$

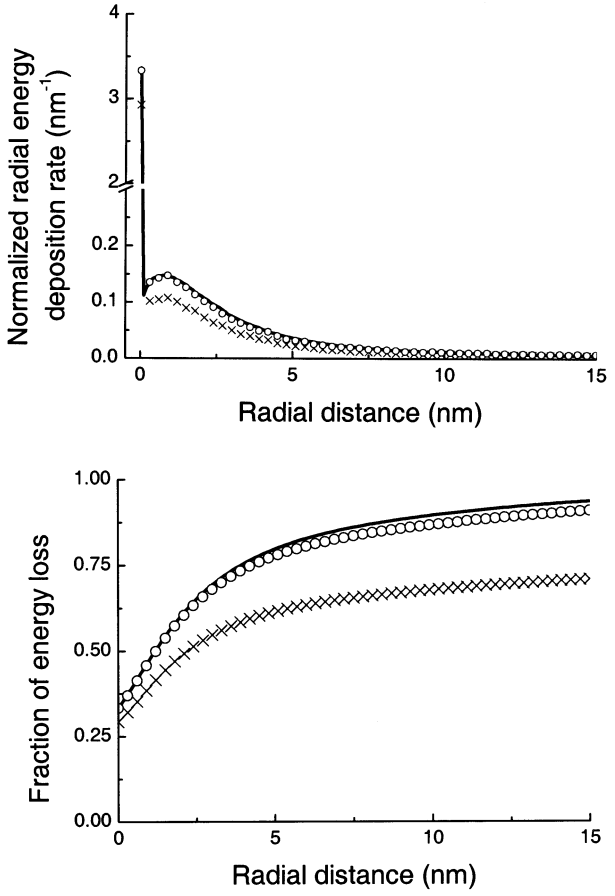

Figure 6. Comparison of the radial energy deposition profile for a 1 MeV ^{1}H (——) in liquid water with those of ^{4}He ions of the same LET (×) and the same velocity (energy per atomic mass unit) (○).

ion of the same velocity, rather than a $^4He^{2+}$ ion of the same LET. Remember that the axial profile is the same for particles of the same mean free path, i.e., LET. Because radiation chemical (and radiobiological) effects depend on the relative locations of the radiation-induced species, this dependence of the radial profile on ion velocity explains the observed deficiencies of LET as a parameter for predicting yields.

To parametrize the effects of radiation quality it is necessary to incorporate the structure of the ion track both in the axial and the radial directions. The mean separation between inelastic collisions determines the axial energy loss rate, and for an ion, A^{Z+}, the mean free path is approximately Z^2 times that of a proton of the same specific energy. Over a reasonable range of primary energies, it may be assumed that the maximum energy of the ejected electrons determines the radial energy loss rate, and this quantity is a function of the specific energy, E/M. Hence, the obvious inference is that an appropriate universal parametrization for radiation chemical effects for energetic, but nonrelativistic ions with energy greater than that corresponding to the Bragg peak is using the parameter $E/(M\,Z^2)$. The effect of particle charge and energy on the differential yield of the Fricke dosimeter using this parametrization, actually its inverse $(M\,Z^2)/E$, is shown in Figure 7. The calculated results for e^-, ^{1}H, ^{4}He, ^{12}C, and ^{20}Ne ions almost lie upon the same curve, dropping from the fast electron limit of 15.6 to ~3.5 ions/100 eV. A decrease to zero is not expected. This value would signify complete recombination of the radiation-induced reactants to H_2O.

As the energy of the incident ion decreases, so does the yield of Fe(III) produced and the yields of the three contributing reactions. In the higher energy regime, 10−100 MeV, the yield

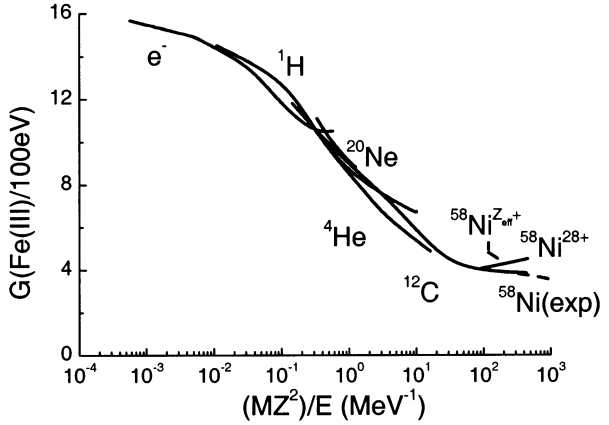

Figure 7. Effect of particle charge and energy on the differential yield of the Fricke dosimeter. IRT simulations employing simulated track structures: (——) labeled curves for ^{1}H, ^{4}He, ^{12}C,^{20}Ne, $^{58}Ni^{Zeff+}$ and $^{58}Ni^{28+}$. Experimental differential yields: LaVerne and Schuler[8] (− − −) ^{58}Ni ions.

of reaction 1 is significantly greater than that of reactions 2 and 3, which have similar yields; however, in the lower energy regime, 0.1−1 MeV, the yields of reactions 1 and 2 are similar and both are greater than that of reaction 3. The change in the importance of the different reactions reflects changes in the nature of the chemistry occurring due to the variation in track structure. At low energy, the separation between energy loss events is small and the radiation-induced clusters of reactants resulting from ionization and excitation of water molecules are close together. Consequently, hydroxyl radicals combine via the intra-track reaction

$$^{\bullet}OH + {}^{\bullet}OH \rightarrow H_2O_2 \quad 2k = 1.1 \times 10^{10}\ M^{-1}s^{-1} \qquad (6)$$

producing hydrogen peroxide. These molecules are then scavenged by Fe(II) according to reaction 2 on a 1−10 s time scale depending on the concentration of Fe(II). The scavenging reaction produces an OH radical, which is immediately scavenged by Fe(II) according to reaction 1. The yields of reaction 1 and reaction 2 are virtually the same suggesting that no OH radicals produced directly by ionization or excitation of water molecules escape from the track and are scavenged by the solute. The thermalization distribution of the hydrated electron is significantly larger than the "fragmentation" distributions of H_2O^+ and H_2O^*. Hydrogen atoms produced directly and by reaction 4 undergo intra-track reaction

$$^{\bullet}H + {}^{\bullet}H \rightarrow H_2 \quad 2k = 1.1 \times 10^{10}\ M^{-1}s^{-1} \qquad (7)$$

or are scavenged by O_2 via reaction 5 to give $HO_2^{\bullet}$. This radical is scavenged by Fe(II) in reaction 3 giving H_2O_2.

At high ion energies, a very different picture holds from that at lower energies because the separation between primary energy events is significantly larger. The inelastic mean free path of a 0.1 MeV $^1H^+$ in liquid water is ~0.9 nm, whereas it is 2.4 nm at 1 MeV, 15.5 nm at 10 MeV, and 100 nm at 100 MeV. The yield of reaction 2 is only slightly larger than the yield of reaction 3, whereas the yield of reaction 1 is much larger than the yield of reaction 2. The implication of these observations is that most of the hydrogen peroxide is produced via reaction 3 and the hydroxyl radicals directly produced by ionization and excitation events do not undergo significant intra-track reaction 6, but escape and are scavenged by Fe(II) according to reaction 1.

The time dependence of G(Fe(III)) has been measured in pulse radiolysis experiments with 20 MeV $^2D^+$ and 39 MeV

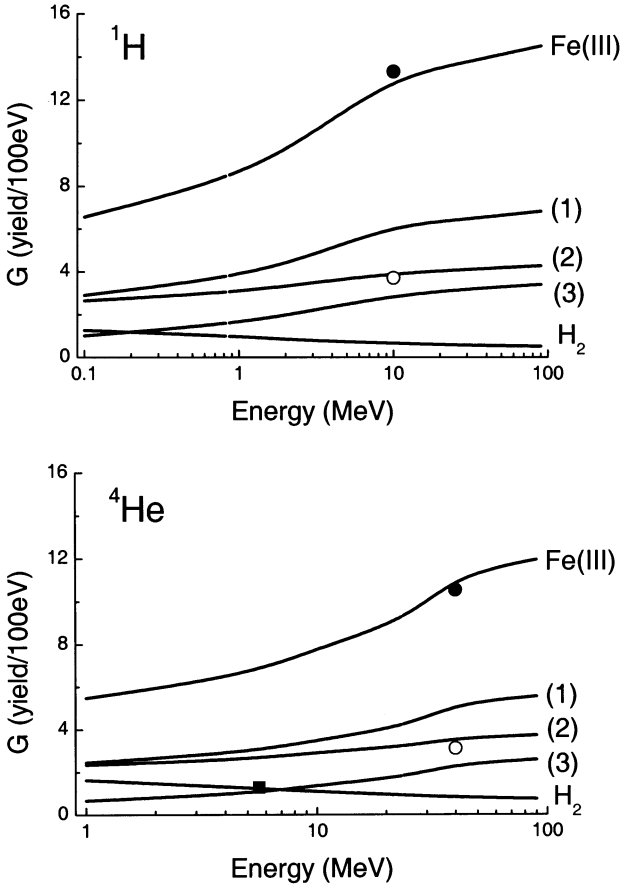

Figure 8. Effect of ion energy on the production of Fe(III), on different reactions resulting in the oxidation of Fe(II) to Fe(III) and on the production of H_2. (——) IRT simulations employing simulated ion track structures. Experiment ^{1}H: (●) G_{total}(Fe(III)),[37] (○) $2G_{slow}$(Fe(III));[37] Experiment ^{4}He: (●) G_{total}(Fe(III)),[37] (○) $2G_{slow}$(Fe(III)),[37] (■) $G(H_2)$.[46]

$^4He^{2+}$ ions.[37] The fast component of the experiments is the sum of the yields of reactions 1 and 3 less the yield of reaction 2, while the slow component is twice the yield of reaction 2. The experimental estimates of the two components are 5.9 and 7.4 for 20 MeV $^2D^+$ and 4.3 and 6.2 for 39 MeV $^4He^{2+}$. The resulting values for the sum (G(reaction (1)) + G(reaction(3))) are 9.6 for 20 MeV $^2D^+$ and 7.4 for 39 MeV $^4He^{2+}$, which are in excellent agreement with the predicted values of 9.1 and 7.5, respectively. The experimental values for G(reaction(2)) and G(Fe(III)) are shown in Figure 8, and are in similarly good agreement with the stochastic diffusion-kinetic predictions.

The yield of molecular hydrogen produced in the radiolysis of the Fricke dosimeter is also shown in Figure 8. This (stable) product is formed by two fundamentally different reactions: (i) by ultrafast subpicosecond formation involving extremely transient species (possibly via dissociative recombination of the water molecular cation, H_2O^+, and a precursor to the hydrated electron, e_{pre}^-), and (ii) by intra-track chemistry via reaction 7. In principle, molecular hydrogen is also formed by the reaction

$$H + Fe(II) + H_3O^+ \rightarrow Fe(III) + H_2 \qquad k = 7.5 \times 10^6\ M^{-1}s^{-1} \quad (8)$$

however, the Fricke dosimeter is an aerated solution. Consequently, the H atoms are scavenged by O_2 and this reaction is negligible, accounting for less than 1% of the hydrogen with the light ions. As the energy of the ion decreases, the separation between inelastic events decreases, which leads to an increase in the amount of intra-track reaction and a decrease in the amount of "escape" and scavenging of radiation-induced reactants from the track. Therefore, the yield of H_2 produced increases with decreasing ion energy. The diffusion-kinetic pathway to H_2 formation via (H + H) reaction accounts for 0.15 molecules/100 eV of the H_2 for 100 MeV ^{1}H, and 0.50 molecules/100 eV for 0.1 MeV ^{1}H. Ultrafast formation yields with ^{1}H are 0.63 molecules/100 eV at 0.1 MeV and 0.36 molecules/100 eV at 100 MeV. Clearly, the physicochemical route to H_2 production is influenced by the track structure, but the change is less significant than observed for diffusion-kinetic formation. This difference is a consequence of the much shorter time scale of the important dissociative recombination reaction

$$H_2O^+ + e_{pre}^- \rightarrow H_2O^* \rightarrow H_2 + O^\bullet \qquad k \approx 2 \times 10^{11}\ M^{-1}s^{-1} \quad (9)$$

which causes a reduced significance of spatial relaxation on the reaction kinetics. Similar effects to those observed in Figure 8 for ^{1}H are also found for ^{4}He (and ^{12}C) ions. The yield of molecular hydrogen produced from the Fricke dosimeter by α particles from ^{210}Po has been determined experimentally[46] and is included in Figure 8. The experimental and calculated values are in good agreement.

For the most part, the agreement between the available experimental data and the predictions of IRT modeling employing simulated track structures is excellent. This good agreement is not found for ^{58}Ni ions. In Figure 2, the IRT calculations for $^{58}Ni^{28+}$ overestimate the yield of Fe(III) by 0.4 ions/100 eV, ~11%, at 200 MeV. This discrepancy is not large, and if the calculation had been performed in isolation, it would have probably been considered acceptable. However, comparison of simulation with experiment over the energy range 100−400 MeV reveals an energy dependence that is incorrect: the simulated G(Fe(III)) decreases with increasing $^{58}Ni^{28+}$ energy, whereas the experimental G(Fe(III)) shows a slight increase with ^{58}Ni ion energy. Unlike the other ions employed by LaVerne and Schuler,[8] ^{58}Ni is not fully stripped over the energy range of the experiments. Over the energy range 100−400 MeV a ^{58}Ni ion in water has an effective charge, Z_{eff}, of ~20+, considerably less than the stripped charge of 28+. Also included in Figure 2 are IRT calculations using ^{58}Ni ion tracks with the appropriate Z_{eff}, evaluated using the approach of Bloom and Sauter.[30] The predictions of these calculations show the correct energy dependence, that is G(Fe(III)) decreases with decreasing ion energy, however, quantitative agreement with the experimental yields is not obtained, with the predicted G(Fe(III)) at 200 MeV being 1.2 ions/100 eV, ~32%, greater than the experimental value. The calculated value of G(Fe(III) is, however, in good agreement with the estimate of Furukawa et al.,[47] ~5.0, that was derived using a model based on the experimental radial dose distribution around a 200 MeV ^{58}Ni ion track. It is merely coincidence that the modeled yield for ^{58}Ni ion tracks with the appropriate Z_{eff} has the same value at 100 MeV as the yield predicted for fully stripped $^{58}Ni^{28+}$.

As the track segment employed in the IRT calculations is sufficiently large that end effects are not important and the calculations have converged, the disagreement between experiment and calculation is significant. Errors in the experimental yields are not believed to be large, especially as the experimental data matches nicely with simulated data for ^{12}C in Figure 7. The discrepancies probably point to fundamental problems in the assumptions involved in constructing the simulated track structures or modeling the radiation induced chemistry. Over

the energy range 100−400 MeV, the mean free path of ^{58}Ni ions is smaller than the effective size of an H_2O molecule in liquid water. The continuum approach to track structure simulation has to breakdown when the mean free path is physically unrealistic. To address this problem, track structure simulations incorporating molecular dynamics simulations for the structure of water are currently in progress. The predictions of the IRT calculations shown in Figure 2 for $^{58}Ni^{Zeff+}$ ions over-estimate the yield of Fe(III). Increasing the mean free path used in the track structure simulations to a physically realistic value (without modifying the energy loss distribution) will increase the separation between radiation-induced radicals and decrease the predicted LET. Furthermore, it ultimately will result in an additional increase in G(Fe(III)). The obvious conclusion is that the formulation used for the energy loss properties of ^{58}Ni ions in water is beginning to breakdown, and the energy loss distribution must be changing with ion energy. Large energy losses and high-energy secondary electrons result from close collisions and so the interacting molecular electron will experience more of the primary ion charge than Z_{eff}. A breakdown in the formulation for the energy loss properties is not unexpected as ^{58}Ni ions in the energy range 100−400 MeV are near the Bragg peak of the stopping power curve. This problem is also under investigation.

Thus far, only problems with the physical model for the track structure have been considered, but deficiencies in the diffusion-kinetic modeling of the chemistry are also present. In the application of the IRT methodology used in the calculations presented here, the solutes and the solvent are treated as a continuum, i.e., deterministically, and they are not depleted by reaction. The track of a ^{58}Ni ion produces an extremely high local concentration of reactants. Consider the simplified case in which the radiation-induced reactants are produced homogeneously in a cylinder of whose radius, r, is the range of a 10 keV electron, that is the most energetic daughter electron possible for a ^{58}Ni ion. The average concentration of reducing radicals is [red] $\approx G(\text{red}) \times LET/(\pi r^2)$, where G(red) is the initial yield of reducing radicals. For 200 MeV ^{58}Ni ions, the LET is $\sim 4.3 \times 10^3$ eV/nm, r is ~ 1.5 μm, G(red) is ~ 5, so [red] ≈ 30 μM. This value is less than an order of magnitude smaller than the concentration of O_2 in aerated solution. As the real volume in which the majority of the reducing radicals are formed is considerably smaller than the volume considered in this simple calculation, the result suggests that depletion of O_2 will be important in determining the yield of the Fricke dosimeter for 100−400 MeV ^{58}Ni ions. Experiments with deaerated solutions give almost the same ferric ion yields as those performed with aerated solutions: at 200 MeV the G-values are 3.2 for deaerated solution and 3.9 for aerated solution. [8] Stochastic IRT calculations using ion tracks with the appropriate Z_{eff} for 200 MeV ^{58}Ni ions predict G(Fe(III)) = 3.6 for deaerated Fricke solution, an error of ~13%. This value is in much better agreement with the experimental yield than is the case for aerated solution where the error is ~32%. Stochastic diffusion-kinetic calculations for the heavy ion radiolysis of the Fricke dosimeter in which the solute species are included explicitly are not computationally feasible given presently available facilities: an exorbitant number of reactants would have to be considered increasing the RAM necessary to an unrealistic level.

Summary

Stochastic simulations of the Fricke dosimeter have been used to investigate the effects of ion track structure on radiation chemical outcome. The simulations accurately reproduce experimentally measured track segment yields for energies in the range 0.1 MeV to 1 GeV for e^-, 1H, ^{4}He, ^{12}C, and ^{20}Ne ions, and are in reasonable agreement for ^{58}Ni ions. Detailed examination of the calculations reveals that at low ion energies, i.e., high LET, there is almost no escape of OH radicals from the ion track, and the yield of Fe(III) is due entirely to scavenging of H_2O_2 formed by the intra-track reaction of ($^\bullet$OH + $^\bullet$OH) and scavenging of $HO_2^\bullet$, which results from the reaction of H atoms with (added) oxygen. In contrast, at higher energies and lower LET, the production of Fe(III) is dominated by the scavenging of OH radicals escaping from intra-track reaction and the scavenging of $HO_2^\bullet$ by Fe(II). The change in the production mechanism is a manifestation of the decrease in the separation between radiation-induced ionization and excitation events with decreasing ion energy. The radical HO_2 contributes to the Fe(III) yield at low ion energies, while the OH radical does not, as $HO_2^\bullet$ is produced by the chain

$$e^-_{pre} \xrightarrow{H_2O} e^-_{aq} \xrightarrow{H_3O^+} H \xrightarrow{O_2} HO_2$$

and the spatial thermalization-solvation distribution of the hydrated electron is significantly broader than the fragmentation distribution of H_2O^+, which is the most significant precursor to $^\bullet$OH.

The LET of the radiation particle in the medium is demonstrated to be a poor parameter for describing the effects of radiation quality on the observed yield of Fe(III). The origins of the failure lie in the structure of the ion track; tracks of different ions with the same LET having different radial profiles. A better parameter for quantifying radiation quality in some radiation chemistry studies is $E/(MZ^2)$; however, it should be recognized that no deterministic parametrization can realistically represent a phenomenon (short-time radiation chemistry) that is stochastic in nature.

Acknowledgment. The authors thank Dr. Marie Begusova for numerous discussions. This is Contribution NDRL-4371 of the Notre Dame Radiation Laboratory. The work described herein was supported by the Office of Basic Energy Sciences of the U.S. Department of Energy.

References and Notes

(1) Zaider, M.; Brenner, D. J. *Radiat. Res.* **1984**, *100*, 245−256.
(2) Turner, J. E.; Hamm, R. N.; Wright, H. A.; Ritchie, R. H.; Magee, J. L.; Chatterjee, A.; Bolch, W. E. *Radiat. Phys. Chem.* **1988**, *32*, 503−510.
(3) Hill, M. A.; Smith, F. A. *Radiat. Phys. Chem.* **1994**, *43*, 265−280.
(4) Pimblott, S. M.; LaVerne, J. A. *J. Phys. Chem.* **1997**, *101*, 5828−5838.
(5) Pimblott, S. M.; LaVerne, J. A. *J. Phys. Chem. A* **1998**, *102*, 2967−2975.
(6) Frongillo, Y.; Goulet, T.; Fraser, M.-J.; Cobut, V.; Patau, J. P.; Jay-Gerin, J.-P. *Radiat. Phys. Chem.* **1998**, *51*, 245−254.
(7) Burns, W. G.; Sims, H. E. *J. Chem. Soc., Faraday Trans. 1* **1981**, *77*, 2803−2813.
(8) LaVerne, J. A.; Schuler, R. H. *J. Phys. Chem.* **1987**, *91*, 5770−5776.
(9) LaVerne, J. A.; Schuler, R. H. In *Radiation Research, Procedings of the 8th International Congress of Radiation Research*; Fielden, E. M., Fowler, J. F., Hendry, J. H., Scott, D., Eds.; Taylor & Francis: London, 1987; Vol. 2, pp 17−22.
(10) LaVerne, J. A.; Schuler, R. H. *J. Phys. Chem.* **1986**, *90*, 5995−5996.
(11) Buxton, G. V.; Greenstock, C. L.; Helman, W. P.; Ross, A. B. *J. Phys. Chem. Ref. Data* **1988**, *17*, 513−886.
(12) Collinson, E.; Dainton, F. S.; Kroh, J. *Proc. R. Soc. London, Ser. A* **1962**, *265*, 422−429.
(13) *Radiation Dosimetry: X-rays Generated at Potentials of 5 to 150 kV*; ICRU Publications: Washington, D. C., 1970; Vol. 17.

(14) *Radiation Dosimetry: Electrons with Initial Energies Between 1 and 50 MeV*; ICRU Publications: Washington, D. C., 1972; Vol. 21.
(15) Katsumura, Y.; Yamamoto, S.; Hiroishi, D.; Ishigure, K. *Radiat. Phys. Chem.* **1992**, *39*, 383−387.
(16) Schwarz, H. A. *J. Phys. Chem.* **1969**, *73*, 1928−1937.
(17) Burns, W. G.; Sims, H. E.; Goodall, J. A. B. *Radiat. Phys. Chem.* **1984**, *23*, 143−180.
(18) Green, N. J. B.; Pilling, M. J.; Pimblott, S. M.; Clifford, P. *J. Phys. Chem.* **1990**, *94*, 251−258.
(19) Green, N. J. B.; Pilling, M. J.; Pimblott, S. M. *Radiat. Phys. Chem.* **1989**, *34*, 105−114.
(20) Pimblott, S. M.; LaVerne, J. A. *Radiat. Res.* **1990**, *122*, 12−23.
(21) Pimblott, S. M.; LaVerne, J. A.; Mozumder, A. *J. Phys. Chem.* **1996**, *100*, 8595−8606.
(22) Ashley, J. C. *J. Electron Spectrosc. Relat. Phenom.* **1988**, *46*, 199−214.
(23) Green, N. J. B.; LaVerne, J. A.; Mozumder, A. *Radiat. Phys. Chem.* **1988**, *32*, 99−103.
(24) Nikogosyan, D. N.; Oraesky, A. A.; Rupasov, V. I. *Chem. Phys.* **1983**, *77*, 131−143.
(25) Crowell, R. A.; Bartels, D. M. *J. Phys. Chem.* **1996**, *100*, 17 940−17 949.
(26) Bartels, D. M.; Crowell, R. A. *J. Phys. Chem. A* **2000**, *104*, 3349−3355.
(27) Green, N. J. B.; Pimblott, S. M. *Res. Chem. Intermed.* **2001**, *27*, 529−538.
(28) Michaud, M.; Sanche, L. *Phys. Rev. A.* **1987**, *36*, 4672−4683.
(29) Michaud, M.; Sanche, L. *Phys. Rev. A.* **1987**, *36*, 4684−4699.
(30) Bloom, S. D.; Sauter, G. D. *Phys. Rev. Lett.* **1971**, *26*, 607−610.
(31) Christman, E. A.; Appleby, A.; Jayko, M. *Radiat. Res.* **1981**, *85*, 443−457.
(32) Gauduel, Y.; Pommeret, S.; Migus, A.; Antonetti, A. *Chem. Phys.* **1990**, *149*, 1−10.
(33) Gauduel, Y.; Pommeret, S.; Migus, A.; Yamada, N.; Antonetti, A. *J. Am. Chem. Soc.* **1990**, *112*, 2925−2931.
(34) LaVerne, J. A.; Pimblott, S. M. *J. Phys. Chem.* **1991**, *95*, 3196−3206.
(35) Clifford, P.; Green, N. J. B.; Oldfield, M. J.; Pilling, M. J.; Pimblott, S. M. *J. Chem. Soc., Faraday Trans.* **1986**, *82*, 2673−2689.
(36) Pimblott, S. M. *J. Phys. Chem.* **1992**, *96*, 4485−4491.
(37) Sauer, M. C.; Hart, E. J.; Naleway, C. A.; Jonah, C. D.; Schmidt, K. H. *J. Phys. Chem.* **1978**, *82*, 2246−2248.
(38) Magee, L.; Chatterjee, A. *Radiat. Phys. Chem.* **1980**, *15*, 125−132.
(39) Magee, J. L.; Chatterjee, A. *J. Phys. Chem.* **1978**, *82*, 2219−2226.
(40) Fulford, J.; Bonner, P.; Goodhead, D. T.; Hill, M. A.; O'Neill, P. *J. Phys. Chem. A* **1999**, *103*, 11 345−11 349.
(41) Allen, A. O. *Radiation Chemistry of Water and Aqueous Solutions*; Van Nostrand: New York, 1961.
(42) Sauer, M. C., Jr.; Schmidt, K. H.; Hart, E. J.; Naleway, C. A.; Jonah, C. D. *Radiat. Res.* **1977**, *70*, 91−106.
(43) Sauer, M. C., Jr.; Jonah, C. D.; Schmidt, K. H.; Naleway, C. A. *Radiat. Res.* **1983**, *93*, 40−50.
(44) Massey, H. S. W.; Burhop, E. H. S. *Electronic and Ionic Impact Phenomena*; Clarendon Press: Oxford, 1952.
(45) Bethe, H. In *Handbuch der Physik*; Geiger, H., Scheel, K., Eds.; Springer: Berlin, 1933; Vol. 24, p 273.
(46) Trumbore, C. N.; Hart, E. J. *J. Phys. Chem.* **1959**, *63*, 867−873.
(47) Furukawa, K.; Ohno, S.-I.; Namba, H.; Taguchi, M.; Watanabe, R. *Radiat. Phys. Chem.* **1997**, *49*, 641−644.